PAPER

Noncontact optical imaging of brain hemodynamics in preterm infants: a preliminary study

To cite this article: Elie G Abu Jawdeh *et al* 2020 *Phys. Med. Biol.* **65** 245009

IOP Publishing Phys. Med. Biol. 65 (2020) 245009 https://doi.org/10.1088/1361-6560/abc5a7

Physics in Medicine & Biology

IPEM Institute of Physics and Engineering in Medicine

PAPER

RECEIVED
24 June 2020

REVISED
6 October 2020

ACCEPTED FOR PUBLICATION
28 October 2020

PUBLISHED
3 December 2020

Noncontact optical imaging of brain hemodynamics in preterm infants: a preliminary study

Elie G Abu Jawdeh[1,6], Chong Huang[2,6], Siavash Mazdeyasna[2], Lei Chen[3], Li Chen[4,5], Henrietta S Bada[1] and Guoqiang Yu[2]

[1] Deparment of Pediatrics/Neonatology, College of Medicine, University of Kentucky, Lexington, KY, United States of America
[2] Department of Biomedical Engineering, College of Engineering, University of Kentucky, Lexington, KY, United States of America
[3] Department of Physiology, College of Medicine, University of Kentucky, Lexington, KY, United States of America
[4] Division of Cancer Biostatistics, Department of Internal Medicine, University of Kentucky, Lexington, KY, United States of America
[5] Biostatistics and Bioinformatics Shared Resource Facility, Markey Cancer Center, University of Kentucky, Lexington, KY, United States of America
[6] Contributed equally as co-first authors.

E-mail: chong.huang@uky.edu

Keywords: preterm infants, brain, cerebral blood flow, diffuse optics, imaging

Abstract

Extremely preterm infants' hemodynamic instability places them at high risk of brain injury. Currently there is no reliable bedside method to continuously monitor cerebral hemodynamics in the neonatal intensive care unit (NICU). This paper reports a feasibility study to adapt and test an innovative speckle contrast diffuse correlation tomography (scDCT) device for noncontact, high-density, 3D imaging of cerebral blood flow (CBF) in preterm infants. The scDCT scans a focused point near-infrared illumination to multiple source positions for deep tissue penetration, and controls an electron multiplying charge-coupled-device camera with thousands of pixels to achieve a high-density sampling. The optimized scDCT for use in preterm infants was first evaluated against an established diffuse correlation spectroscopy in an infant-head-simulating phantom with known properties. The observed significant correlation between the two measurements verified the capability of scDCT for transcranial brain imaging. The insignificant influence of transparent incubator wall on scDCT measurements was then confirmed by comparing adult forearm blood flow responses to artery cuff occlusions measured inside and outside the incubator. Finally, the scDCT device was moved to the NICU to image CBF variations in two preterm infants. Infant #1 with no major organ deficits showed little CBF fluctuation over the first 3 weeks of life. Infant #2 showed a significant CBF increase after the 2 h pharmacotherapy for patent ductus arteriosus closure. While these CBF variations meet physiological expectations, the fact that no significant changes are noted with peripheral monitoring of blood oxygen saturation suggests necessity of direct cerebral monitoring. This feasibility study with timely technology development is an important and necessary step towards larger clinical studies with more subjects to further validate it for continuous monitoring and instant management of cerebral pathologies and interventions in the NICU.

1. Introduction

Approximately 15 million children are born prematurely in the world every year (Blencowe *et al* 2013). Survival rates for preterm infants have improved dramatically in recent decades due to advances in perinatal and neonatal care (Hinojosa-Rodriguez *et al* 2017). However, this reduction in mortality has not translated into a comparable reduction in neuro-developmental morbidity. Approximately one half of extremely preterm infants suffer from neurofunctional impairments in a broad range of motor, cognitive, and

behavioral domains, thus placing a significant burden on families and society. Major contributors to their brain injury and hemorrhage are frequent fluctuations in cerebral blood flow (CBF) and cerebral oxygenation superimposed on an immature brain structure and function (Noori and Seri 2015). As new interventions and bundles are developed to reduce brain injury, a reliable noninvasive method for frequently assessing cerebral hemodynamics at the bedside in the neonatal intensive care unit (NICU) is imperative.

Currently, clinicians rely mainly on techniques that indirectly measure cerebral perfusion (e.g. blood pressure, pulse oximetry) for day-to-day management in the NICU. While recent neuroimaging researches using cranial ultrasonography (Park *et al* 2015) and magnetic resonance imaging (MRI) (Wang *et al* 2018) have provided better understanding of structural alterations associated with adverse neurodevelopmental outcomes in preterm infants, prediction of later functional disability remains modest. Moreover, large neuroimaging tools such as MRI are not practical for frequent use due to their size and cost.

Near-infrared spectroscopy (NIRS) and relevant tomography technologies have been used for decades as noninvasive bedside tools for continuous monitoring of cerebral oxygenation (Zaramella *et al* 2006, Underwood *et al* 2007, Naidech *et al* 2008, Hyttel-Sorensen *et al* 2013, 2015, Severdija *et al* 2015, Greisen *et al* 2016, Banerjee *et al* 2016, Chock *et al* 2016, Kooi *et al* 2017). Another recently developed dynamic NIRS method, diffuse correlation spectroscopy (DCS), provides noninvasive CBF measurements (Boas *et al* 1995a, Boas and Yodh 1997, Shang *et al* 2009, 2011, 2014, Buckley *et al* 2009, Kim *et al* 2010, Durduran *et al* 2010, Cheng *et al* 2012a, 2014). However, most systems lack the combination of spatial resolution and wide field-of-view (FOV) to image spatially distributed brain functions and discriminate the brain signal from overlaying scalp and skull. A few high-density tomographic systems use numerous discrete sources and detectors coupled with fiber bundles to a head cap (Hebden *et al* 2002, White *et al* 2012, Ferradal *et al* 2016). However, adjusting and maintaining a stable optical coupling of numerous fibers to a small fragile neonatal head (i.e. *a contact measurement*) is labor-intensive and poses great challenges to head cap design with safety concern.

Recent development of a near-infrared (NIR) speckle contrast diffuse correlation tomography (scDCT, US Patent #9 861 319, 2016–2036) (Yu *et al* 2016) provides a noninvasive noncontact optical tool for fast and high-density 3D imaging of CBF distributions deeply into brains of rodents and neonatal piglets (Huang *et al* 2015a, 2017, 2019b, Yu *et al* 2016). This paper demonstrates the feasibility of adapting this innovative device for noncontact 3D imaging of CBF distributions in preterm infants through the transparent incubator wall in the NICU. An infant-head-simulating phantom with known optical properties were used to verify the transcranial ability of scDCT against an established DCS. The incubator wall impact on the scDCT measurement was evaluated by imaging forearm blood flow responses to artery cuff occlusions inside and outside the incubator. Finally, the feasibility of scDCT use in the NICU was demonstrated by imaging CBF variations in two preterm infants.

2. Methods

2.1. scDCT technology for 3D imaging of neonatal CBF

Details about the scDCT technology can be found in our previous publications (Yu *et al* 2016, Huang *et al* 2017, 2019b, Mazdeyasna *et al* 2018). As shown in figure 1(a), an electrically controlled galvo mirror (step response time: 300 μs) scans coherent point light at 785 nm (DL785-100-S, coherence length >10 meters, CrystaLaser) to multiple source positions on an adjustable region of interest (ROI). The power of incident light from the scDCT on tissue surface is <0.5 mW (measured by a power meter), which meets Accessible Emission Limit Class 3R of American National Standards Institute standard (<5 mW) for safety. An electron multiplying charge-coupled devices camera (pixels: 1002 × 1004; frame rate: 8 Hz, cascade 1 K, Photometrics) is used to detect spatial speckle contrasts resulting from motion of moving scatterers (e.g. red blood cells) in the selected ROI. A zoom lens (Zoom7000, Navitar) enables selection of the ROI and working distance. The F number of the zoom lens was set to 8 to make the sensing meet Nyquist sampling criteria (Boas and Dunn 2010). A long-pass filter (>750 nm, Edmund Optics) is installed in front of the zoom lens to reduce ambient light. A pair of crossed linear polarizers are setting across the source and detector paths respectively to block direct reflected rays from the source.

In the present study to balance the tempo-spatial resolution and ROI, 25 source positions were scanned over an ROI of 40 × 40 mm^2 on infant's forehead, which took about 20 s in total. The raw images were collected via sequencing the source positions by the galvo mirror. Four frames were taken at each source location for averaging to improve signal-to-noise ratio (SNR). Noises were first corrected from the raw images including dark noise, shot noise, and the smear effect caused by frame transfer process (Huang *et al* 2015a, 2017). The spatial speckle contrast $K_s(r)$ was quantified by calculating the light intensity ratio of standard deviation (σ_s) and mean $\langle I \rangle$: $K_s(r) = \sigma_s / \langle I \rangle$ in a defined detector on the camera that consisted of 7 × 7 pixels at an area of 0.05 × 0.05 mm^2. $K_s(r)$ values in adjacent 3 × 3 detectors were then spatially

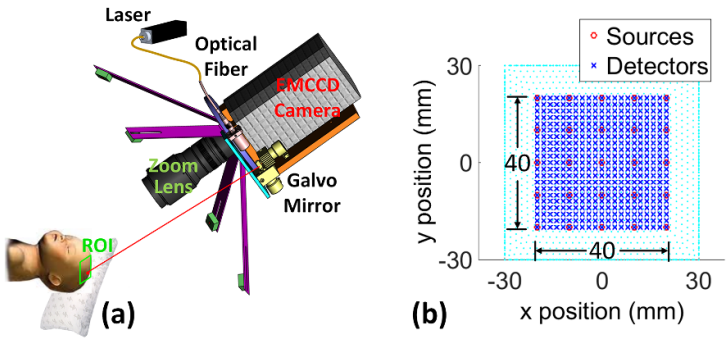

Figure 1. Schematic of scDCT system. (a) Experimental setup for imaging an infant head. (b) Source-detector (S-D) arrangement within the ROI of 40 × 40 mm^2. The 5 × 5 sources (circles) and 21 × 21 detectors (crosses) were evenly distributed on the surface of the ROI to acquire boundary blood flow index data for 3D image reconstruction.

averaged to further improve SNR. A blood flow index ($BFI(r)$) at each source-detector (S-D) pair on the measured tissue boundary was then extracted through a nonlinear relation between the boundary $BFI(r)$ and $K_s(r)$ (Huang *et al* 2017).

As shown in figure 1(b), 21 × 21 detectors were defined in the selected ROI for 3D image reconstruction. With this S-D configuration, the distance between two adjacent detectors was 2 mm, which allowed arrangement of 441 detectors without overlaps in the ROI on the infant's forehead. The boundary BFIs obtained from the effective S-D pairs ranging from 7 to 17 mm were used for image reconstruction, according to our previous testing results (Huang *et al* 2017). Based on photon diffusion theory, penetration depth of NIR light into biological tissues is approximately one half of the S-D distance (Irwin *et al* 2011, Huang *et al* 2017). Therefore, the selected S-D pairs allow to catch photons from a maximum depth of ∼10 mm, reaching the infant brain.

The boundary BFIs were then implanted into a modified near-infrared fluorescence and spectral tomography program that was developed previously by our group for expedient finite-element-method (FEM)-based scDCT tomographic reconstructions (Lin *et al* 2014, Huang *et al* 2015a, 2017). The image reconstruction was processed in a 60 × 60 × 30 mm^3 slab with total mesh nodes of 20 K. The relative CBF (rCBF) at each mesh node (light blue dots in figure 1(b)) was calculated by normalizing the BFIs to its baseline value before physiological changes. Images are displayed with ParaView (Kitware), an open source visualization tool.

2.2. Experimental design

2.2.1. Infant-head-simulating phantom tests

To address whether scDCT can be performed transcranially through the infant skull, we conducted comparison flow measurements against the established conventional DCS in an infant-head-simulating phantom (figure 2(a)). An infant skull (31 weeks after fertilization, from Evolution Store) was inverted and filled with a liquid tissue phantom that consisted of distilled water, India ink (Black India) and Intralipid particles (Fresenius Kabi). Concentration of Intralipid particles controls light scattering while concentration of India ink controls light absorption. Brownian motion of Intralipid particles inside the liquid phantom mimic diffusive movements of red blood cells (i.e. blood flow) in a bulk tissue volume (Boas *et al* 2016). Based on phantom recipe, baseline optical properties of the Intralipid phantom at the room temperature were set as: absorption coefficient $\mu_a = 0.05$ cm^{-1} and reduced scattering coefficient $\mu_s' = 8$ cm^{-1} at the wavelength of 785 nm. These optical properties at 785 nm were close to the reported values in the infant brain measured at 788 nm ($\mu_a = 0.078$ cm^{-1} and $\mu_s' = 9.16$ cm^{-1}) (Zhao *et al* 2005).

Data were collected concurrently by the noncontact scDCT from the outer skull surface, and a contact fiber-optic DCS probe placed directly on the surface of interior liquid phantom through the foramen magnum. For the scDCT measurements, the ROI was reduced to 30 × 30 mm^2 to adapt the small area of infant frontal skull. The skull thickness at the ROI was ∼2 mm. Details for the DCS technology can be found in previous publications (Boas *et al* 1995a, Boas and Yodh 1997, Cheung *et al* 2001, Durduran *et al* 2010, Huang *et al* 2015b, 2015c, Agochukwu *et al* 2017). The DCS device used in this study consists of a long-coherence-length (>10 m) NIR laser diode (785 nm, 100 mW, CrystaLaser), a single-photon-counting avalanche photodiode (APD, Perkin Elmer), and a correlator board (correlator.com). Coherent light is delivered to the phantom through a multimode source fiber (diameter: 200 μm) coupled to the laser diode. The motion of moving Intralipid particles in the liquid phantom results in light intensity fluctuation, which is collected by a single-mode detector fiber (diameter: 5 μm) coupled to the APD. The detected temporal

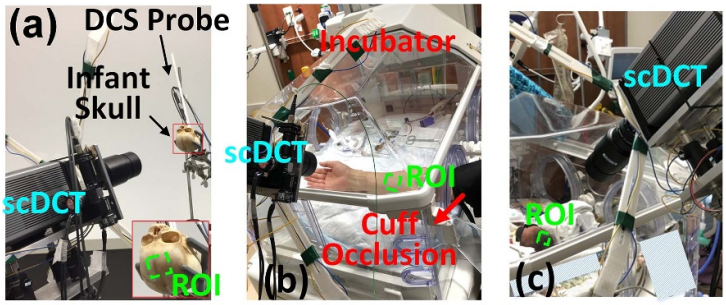

Figure 2. Experimental setups to test the scDCT. (a) Test of scDCT with the infant-head-simulating phantom against DCS. The scDCT scanned over an ROI of 30 × 30 mm^2 on the frontal head of the infant skull. A DCS probe was installed on the surface of Intralipid phantom through foraman magnum. (b) Test of scDCT with the human forearm through the incubator wall, with an ROI of 40 × 40 mm^2 on the forearm. (c) Test of scDCT with an infant in the NICU, with an ROI of 40 × 40 mm^2 on the infant head.

intensity fluctuation is input to the correlator, yielding an autocorrelation curve. Blood flow index is extracted by fitting the autocorrelation curve, whose decay rate depends mainly on motion of moving Intralipid particles. For comparisons, the S-D separation in the DCS is set as 15 mm to match the S-D range of 7–17 mm used in the scDCT.

The Intralipid particle flow was manipulated by changing phantom temperature from 48 °C to room temperature (23 °C). Particle flow was intermittently measured at six temperatures with each measurement of ∼1.5 min. Data were normalized as relative flow to the step of room temperature (23 °C) and presented as percentage changes. Pearson's correlation coefficient and corresponding 95% confidence interval (CI) were calculated to investigate correlations between the scDCT and DCS measurements. A value of $p < 0.05$ was considered a statistically significant correlation between the two measurements.

2.2.2. In-vivo *adult forearm tests*

This *in-vivo* test was approved by the University of Kentucky (UK) Institutional Review Board (IRB). The written IRB consent was obtained before participation. One healthy adult participated in this pilot study.

To assess the impact of transparent incubator wall to blood flow measurements, we tested our scDCT for continuous imaging of blood flow changes during artery cuff occlusion in an adult forearm measured inside and outside the incubator in the NICU (figure 2(b)). The occlusion protocol included a 4 min baseline, a 4 min artery cuff occlusion, and a 4 min recovery. A tourniquet with a pressure of 230 mmHg was applied on the upper arm to occlude blood flow to the forearm. Continuous imaging was performed in the ROI of 40 × 40 mm^2 on the forearm. Data were normalized to the baseline and presented as relative percentage change of blood flow (rBF). Pearson's correlation coefficient and corresponding 95% CI were calculated to investigate correlations between the two scDCT measurements inside and outside the incubator. A value of $p < 0.05$ was considered a statistically significant correlation between the two measurements.

2.2.3. In-vivo *neonatal brain tests*

With IRB approval of UK, two extremely preterm infants were imaged by scDCT through transparent incubator wall (figure 2(c)). Infant #1 was born at 25 1/7 weeks gestation with the birth weight of 815 grams, and imaged at 1, 2, and 3 weeks of life. Infant #2 was born at 26 5/7 weeks gestation with birth weight of 995 grams, imaged at 8 days-of-life during patent ductus arteriosus (PDA) pharmacotherapy. Infant #2 was imaged at the beginning and after 2 h indomethacin treatment for PDA closure. The rationale for Infant #2 was to measure changes in rCBF associated with PDA constriction from treatment. Both subjects were male with no significant complications.

The sleeping infant was continuously imaged by the scDCT over ∼5 min during each measurement (figure 2(c)). The reconstructed CBF values at different time points were normalized to the first measurement (as the baseline) to obtain rCBF. No motion artifacts were observed during each of the measurements over the short period of 5 min. One-way ANOVA was used to compare rCBF values at 1, 2 and 3 weeks of life for Infant #1. Student's t-test was used to compare rCBF values before and after the pharmacotherapy for Infant #2. A value of $p < 0.05$ was considered a statistically significant difference.

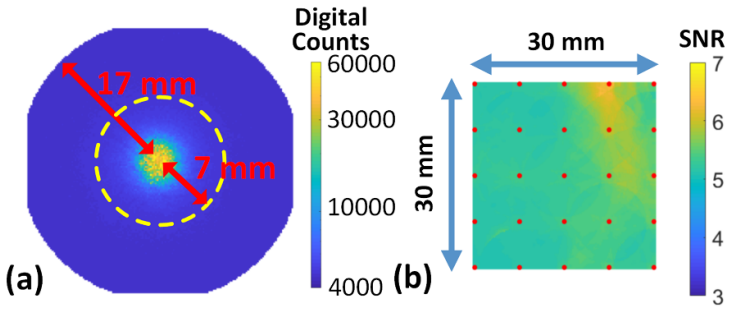

Figure 3. Distributions of digital electrical counts (I) in log scale (a) and SNRs (b), measured by the scDCT in the infant-head-simulating phantom.

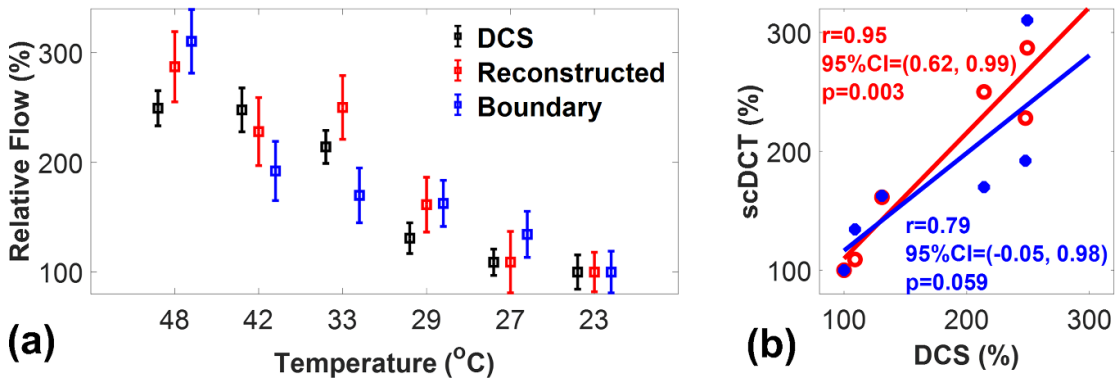

Figure 4. Testing results of the scDCT against DCS in the infant-head-simulating phantom. (a) The Intralipid particle flow (mean ± standard deviation) decreases with the decrease of phantom temperature. The error bars represent temporal variations in scDCT and DCS, respectively, over the period of 5 min in each measurement. (b) Scatter plot of boundary (solid blue dots) and reconstructed (circle red dots) flow data of scDCT against the DCS flow data. The blue and red lines are fitted by linear regression. r represents Pearson's correlation coefficient.

3. Results

3.1. Infant-head-simulating phantom test results

Figure 3(a) shows digital electrical count (I) distribution in the infant-head-simulating phantom, measured by the detectors located at 0–17 mm away from the central source. The averaged digital counts were 59 172 and 4128 at S-D separations of 0 mm and 17 mm, respectively, which are much higher than the average dark count (808) of the camera. The SNR was calculated by the I/I_{noise}, where I_{noise} denotes the dark noise intensity of the camera. Figure 3(b) shows averaged SNR distribution across all effective S-D pairs with the separations of 7–17 mm. The SNRs distributed evenly ranging from 5.1 to 6.4, which were sufficient for extracting flow information, based on our previous study (Huang *et al* 2019a).

Figure 4(a) shows the reduction of Intralipid particle flow with the decrease of temperature, quantified concurrently by the scDCT and DCS devices. Average results in the boundary flow and reconstructed flow at the depth of 5 mm by the scDCT were compared respectively to the 'true flow' values measured by the DCS. As expected, a better correlation against DCS flow was observed (figure 4(b)) with the reconstructed flow from the deep 'brain' (Pearson's correlation coefficient $r = 0.95$, 95%CI = (0.62, 0.99), and $p = 0.003$), compared to the boundary flow without correction of partial volume artifact from the skull ($r = 0.79$, 95%CI = (−0.05, 0.98), and $p = 0.059$).

3.2. *In-vivo* adult forearm test results

Figure 5(a) displays reconstructed rBF images at the baseline (T1), artery cuff occlusion (T2), reactive hyperemia (T3), and recovery period (T4); data were acquired by scDCT through transparent incubator wall and in free space. Figure 5(b) shows comparison of rBF changes in time course at the center of tissue volume (blue dot in figure 5(a)), measured inside and outside the incubator, respectively. Although variations exist, time-course changes in rBF agreed very well (figure 5(c)) between the two measurements ($r = 0.91$, 95%CI = (0.78, 0.96), $p < 10^{-5}$).

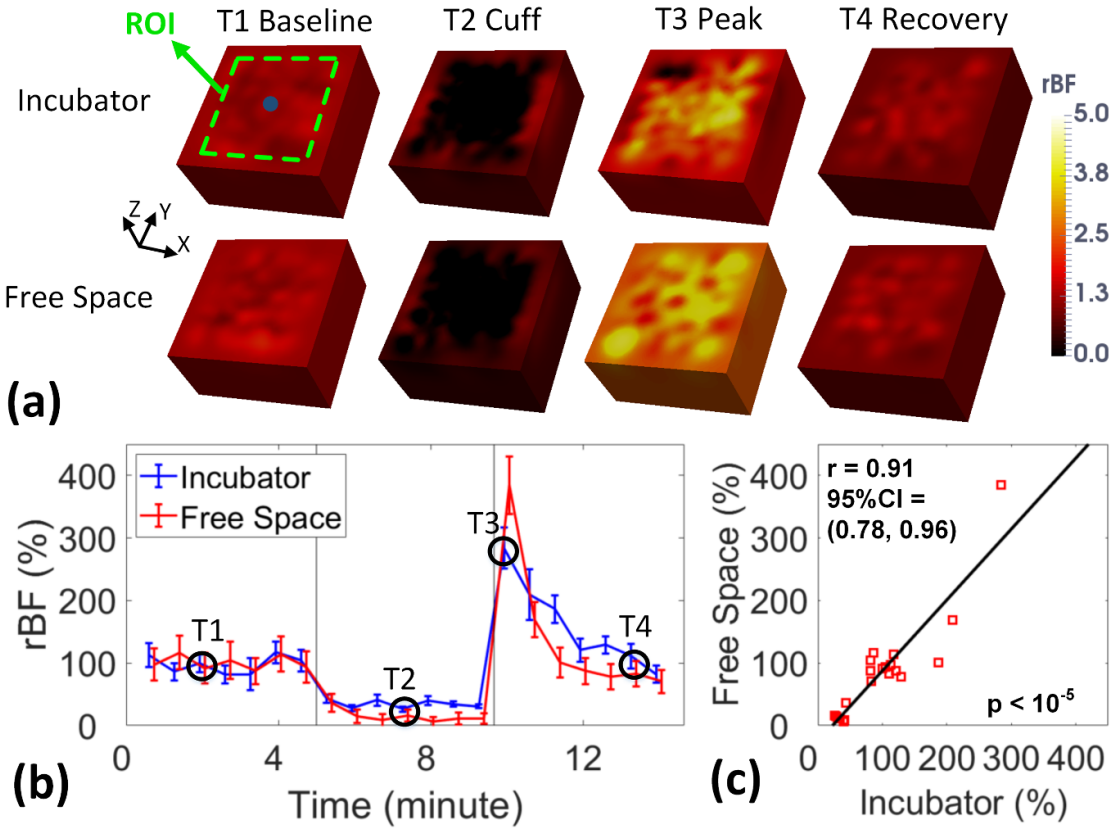

Figure 5. Testing results of the scDCT in an adult forearm during artery cuff occlusion. (a) Reconstructed rBF images at baseline (T1), artery cuff occlusion (T2), reactive hyperemia (T3), and recovery period (T4), measured through incubator wall (top) and in free space (bottom), respectively. (b) Comparison of time-course changes in rBF (mean ± standard deviation), measured through incubator wall (blue curve) and in free space (red curve), respectively. The error bars represent spatial variations over the selected nodes in the central blue dot. (c) Scatter plot of scDCT data, obtained through incubator wall and in free space. The solid line is fitted by linear regression. r represents Pearson's correlation coefficient.

3.3. *In-vivo* neonatal brain test results

Figure 6(a) shows the cross-sectional views of 3D images of reconstructed rCBFs at the depths of 6 mm in week 1 to week 3 measurements of Infant #1. The Infant #1 shows little variations in rCBF over the first 3 weeks of life, with mean ± standard deviation among images of 100.0 ± 1.4%, 98.4 ± 1.1%, and 99.6 ± 1.6%. No significant difference was found among measurements at 1, 2, and 3 weeks of life (one-way ANOVA, $p = 0.14$).

Figure 6(b) shows the cross-sectional views of 3D images of reconstructed rCBFs at the depths of 6 mm before and after the pharmacotherapy of Infant #2. Infant #2 shows a significant increase in rCBF, with mean ± standard deviation among images of 100.0 ± 5.4% and 110.5 ± 3.8%, respectively before and after the pharmacotherapy. Infant #2 shows a significant increase in rCBF (Student's t-test, $p = 0.0003$) between the measurements before and after the pharmacotherapy. The rCBF increase corresponded to a significant increase in blood pressure from 51/25 to 59/31 mmHg after the 2 h PDA pharmacotherapy. No significant changes were noted in peripheral oxygen saturation, measured by a finger pulse oximetry.

4. Discussion and conclusions

4.1. Study motivations and innovations

To date, there is no established bedside method for continual monitoring of cerebral hemodynamics to guide day-to-day management in NICUs. NIRS/DCS technologies have been used at the bedside of clinics for continuous measurements of cerebral oxygenation and CBF variations (Yu *et al* 2003, Cheng *et al* 2012a, Scholkmann *et al* 2014, Buckley *et al* 2014, Durduran and Yodh 2014, Jain *et al* 2014, Lynch *et al* 2014). However, most systems lack the combination of temporal/spatial resolution and wide FOV sufficient to rapidly image distributed brain functions. As every measurement is a mixture of hemodynamics occurring in multiple tissue layers (scalp, skull, brain), it is difficult to discriminate the brain signal of interest. Recent advances in application of high-density diffuse optical tomography systems have largely improved spatial resolution and better separation of cerebral signals from superficial confounds (Hebden *et al* 2002, White

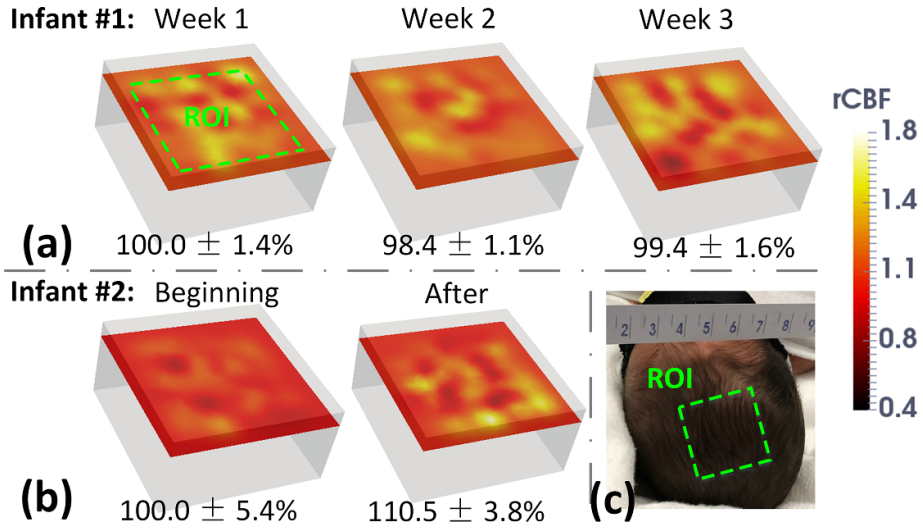

Figure 6. Testing results of the scDCT in two extremely preterm infants. (a) Slight variations in rCBF were observed over the 3 weeks of life in Infant #1. (b) A significant elevation in rCBF was observed after pharmacotherapy, correlating with an increase in blood pressure, in Infant #2. The reconstructed images of rCBF values shown in (a) and (b) were from only one layer at the depth of 6 mm beneath the scalp. Standard deviation represents temporal variations over 5 min in each measurement. (c) An ROI of 40 × 40 mm^2 was selected on the infant's head for boundary data collection, which corresponded to the ROI in the reconstructed image (a).

et al 2012, Ferradal *et al* 2016). However, expanding the FOV to cover a significant portion of the head introduces great challenges in expensive high-channel-count instrumentation, difficult fiber-optic-scalp contact coupling, and complex data quality management. Particularly, adjusting and maintaining a stable optical coupling of numerous rigid and fragile optical fibers to a small neonatal head is labor-intensive and poses significant challenges on head cap design (Hebden *et al* 2002, White *et al* 2012, Ferradal *et al* 2016). These challenges are particularly difficult to overcome when adopting these contact measurement systems to small and fragile heads of preterm infants for continuous and longitudinal monitoring.

Our novel scDCT technique presented in this manuscript provides many unique advanced features over these NIR based technologies, which may impact current basic neuroscience research and clinical neonatal applications. These advanced features include fully noncontact hardware, rapid data acquisition, high-sampling density (using a camera), adjustable S-D patterns/density for high-resolution imaging over a flexible FOV, FEM-based image reconstruction of objects with arbitrary geometries, and a simple low-cost ergonomic instrument. The innovative noncontact hardware design not only eliminates probe-tissue interaction/infection but also avoids the difficulty of cap/helmet fitting on the fragile neonatal infant head, which is also time consuming. The 3D reconstruction of blood flow distribution allows for correcting partial volume effects on the brain from the overlaying tissues (scalp and skull).

4.2. Interpretation of test results in the infant-head-simulating phantom and adult forearm

The goal of the present study was to adapt and test the scDCT for cerebral imaging of preterm infants in the NICU. To achieve the goal, we optimized the S-D configuration and ROI to balance the tempo-spatial resolution and wide FOV (figures 1 and 2). For validation, we conducted concurrent measurements by the scDCT and established DCS in an infant-head-simulating phantom with known optical properties and skull thickness (figures 3 and 4). Significant correlations were observed between the two measurements, verifying the capability of scDCT for transcranial brain imaging. Compared to the boundary flow, which is a mixture signal of skull and brain (Intralipid solution), 3D reconstructed flow in the brain (at the depth of 5 mm) shows a better correlation with the true brain flow, measured directly on the liquid phantom (mimicking brain) by the DCS. This result demonstrates the effectiveness of 3D reconstruction for correcting the partial volume effect from skull.

We notice that there were reported small variations in phantom optical properties (μ_a and μ_s') due to the temperature change (Cletus *et al* 2010). In the future we may include concurrent measurements of optical properties (by standard NIRS devices) and Intralipid particle flow in tissue phantoms to precisely evaluate the influence of optical properties on scDCT measurements.

Another challenge with the use of scDCT in the NICU is to take noncontact optical measurements through the wall of the incubator (for maintaining thermoregulation in preterm infants) without touching the infant. The goal of the designed artery cuff occlusion experiment was to test the potential impact of

transparent incubator wall on noncontact scDCT measurements. Artery cuff occlusion has been extensively used to test NIRS/DCS devices in detecting dynamic changes in tissue hemodynamics (Yu *et al* 2007, Gurley *et al* 2012, Shang *et al* 2013). The observed consistent rCBF responses during artery occlusions inside and outside the incubator (figure 5) suggested insignificant impact of incubator wall on scDCT measurements. Furthermore, the forearm blood flow variations during artery cuff occlusion were found to agree well with those measured previously by DCS devices (Yu *et al* 2007, Gurley *et al* 2012, Shang *et al* 2013).

4.3. Interpretation of test results in the preterm infants

Encouraged by the success of preliminary evaluations in the phantom and forearm, we tested the feasibility of scDCT for imaging of CBF variations in two preterm infants in the NICU. Results from infant #1 (figure 6(a)) with no major organ deficits showed expected little fluctuation in rCBF over the first 3 weeks of life. Results from Infant #2 (figure 6(b)) undergoing pharmacotherapy for PDA closure showed a significant rCBF increase, which might be associated with the reduction of flow steal by PDA constriction. Moreover, rCBF elevation in Infant #2 also corresponded to the increase in blood pressure. To further investigate whether there is a significant increase in rCBF after pharmacotherapy for the general infant population, studies on a cohort of infants need to be conducted in the future. While these dynamic changes in rCBF meet physiological expectations, the fact that no significant changes are noted with peripheral monitoring of blood oxygen saturation suggests necessity of direct cerebral monitoring.

4.4. Study challenges, limitations, and perspectives

While excited about our preliminary results, we recognize challenges and limitations in this pilot study. One major limitation is the small number of subjects. However, we believe this feasibility study with timely technology development is an important and necessary step towards larger clinical studies that would enroll more subjects to further validate the innovative scDCT technique against gold standards.

There are some technological challenges to be overcome, including potential head motion artifacts and influences from the head geometry and hairs. Our noncontact scDCT was designed for frequent checking of CBF variations through the wall of a close incubator to minimize districting preterm infants. Since preterm neonates slept majority of time, we did not observe motion artifacts during our measurements in 5 min. This was one of the reasons that we chose preterm infants to test our scDCT over a short period of time (5 min). In the future, we plan to use a video camera to continuously track head motions during scDCT measurements. If images become corrupted by the motion, these will be excluded, and additional images will be taken to compensate for loss.

Moreover, we have recently integrated a novel photometric stereo technology to our scDCT system to obtain head surface geometry for CBF image reconstruction in heads with arbitrary geometry (Mazdeyasna *et al* 2018). To reduce the hair influence on scDCT measurements, we may reduce the detector size on the camera and increase the sampling density with a larger pixel number of camera to collect more photons between hairs.

Supported by the National Institutes of Health, we are currently working in neonatal piglets to address these potential influences. We are also working on the calibration of scDCT against standard perfusion MRI in both piglets and preterm infants to obtain absolute CBF measurements. Furthermore, scDCT will be extended to a multiple-wavelength system to image both CBF and cerebral blood oxygenation, which allows for the derivation of cerebral oxidative metabolism.

4.5. Conclusions

This pilot study tested our innovative scDCT system for 3D imaging of CBF in preterm infants. With the optimized ROI and S-D arrangement, the infant-head-simulating phantom test against the established DCS verified the capability of scDCT for transcranial brain imaging. The comparison between measurements of human forearm blood flow inside and outside the incubator resulted in well agreed blood flow changes, demonstrating an insignificant influence of the incubator wall. Two infants were tested in the NICU; Infant #1 without major organ deficits showed expected little fluctuation in rCBF during 3 weeks of life, while Infant #2 undergoing pharmacotherapy for PDA closure showed an expected significant rCBF increase. Although our scDCT is not designed for continuous cerebral monitoring, it can be easily used at the bedside of clinics to frequently check CBF level/variation, a major factor impacting the brain function in preterm infants. In the future, our noncontact scDCT may be used more frequently (at more time points) for rapid neonatal brain assessment and management.

Preterm infants are ideal candidates for the use of noncontact scDCT because they have: (1) thin skulls, which are easily penetrated through by the scDCT; (2) unstable cerebral hemodynamics due to frequent bradycardia and oxygen desaturations events on top of often impaired cerebral autoregulation; and (3) immature skin that may be sensitive to pressure, friction or heat accumulation with contact measurement

options. Ultimately, we anticipate that such noninvasive, noncontact, frequent, and longitudinal cerebral monitoring tools, will be able to guide clinicians during therapeutic interventions and will have both diagnostic and prognostic applications in the NICU.

Acknowledgments

This work was supported in part by the National Institute of Health (R21-HD091118, R01-HD101508, R01-AG062480, R01-EB028792, and R56-NS117587) and National Science Foundation (EPSCoR#1539068). We thank the support of the NICU research staff and nurses at University of Kentucky.

Conflict of interest

The authors have no conflict of interests to declare.

ORCID iDs

Elie G Abu Jawdeh https://orcid.org/0000-0003-4414-7007
Chong Huang https://orcid.org/0000-0002-5260-9112
Siavash Mazdeyasna https://orcid.org/0000-0001-5683-9866

References

Agochukwu N B, Huang C, Zhao M, Bahrani A A, Chen L, Mcgrath P, Yu G and Wong L 2017 A novel noncontact diffuse correlation spectroscopy device for assessing blood flow in mastectomy skin flaps: a prospective study in patients undergoing prosthesis-based reconstruction *Plast. Reconstr. Surg.* **140** 26–31

Banerjee J, Leung T S and Aladangady N 2016 Cerebral blood flow and oximetry response to blood transfusion in relation to chronological age in preterm infants *Early Hum. Dev.* **97** 1–8

Blencowe H, Cousens S, Chou D, Oestergaard M, Say L, Moller A B, Kinney M Lawn J and Born Too Soon Preterm Birth Action G 2013 Born too soon: the global epidemiology of 15 million preterm births *Reprod Health* **10** S2

Boas D A, Campbell L E and Yodh A G 1995 Scattering and imaging with diffusing temporal field correlations *Phys. Rev. Lett.* **75** 1855–8

Boas D A and Dunn A K 2010 Laser speckle contrast imaging in biomedical optics *J. Biomed. Opt.* **15** 011109

Boas D A, Sakadzic S, Selb J, Farzam P, Franceschini M A and Carp S A 2016 Establishing the diffuse correlation spectroscopy signal relationship with blood flow *Neurophotonics* **3** 031412

Boas D A and Yodh A G 1997 Spatially varying dynamical properties of turbid media probed with diffusing temporal light correlation *J. Opt. Soc. Am.* A **14** 192–215

Buckley E M *et al* 2009 Cerebral hemodynamics in preterm infants during positional intervention measured with diffuse correlation spectroscopy and transcranial Doppler ultrasound *Opt. Express* **17** 12571–81

Buckley E M, Parthasarathy A B, Grant P E, Yodh A G and Franceschini M A 2014 Diffuse correlation spectroscopy for measurement of cerebral blood flow: future prospects *Neurophotonics* **1** 011009

Cheng R, Shang Y, Hayes D Jr. , Saha S P and Yu G 2012 Noninvasive optical evaluation of spontaneous low frequency oscillations in cerebral hemodynamics *NeuroImage* **62** 1445–54

Cheng R, Shang Y, Wang S Q, Evans J M, Rayapati A, Randall D C and Yu G 2014 Near-infrared diffuse optical monitoring of cerebral blood flow and oxygenation for the prediction of vasovagal syncope *J. Biomed. Opt.* **19** 017001

Cheung C, Culver J P, Takahashi K, Greenberg J H and Yodh A G 2001 In vivo cerebrovascular measurement combining diffuse near-infrared absorption and correlation spectroscopies *Phys. Med. Biol.* **46** 2053–65

Chock V Y, Rose L A, Mante J V and Punn R 2016 Near-infrared spectroscopy for detection of a significant patent ductus arteriosus *Pediatr. Res.* **80** 675–80

Cletus B, Kunnemeyer R, Martinsen P and Mcglone V A 2010 Temperature-dependent optical properties of Intralipid® measured with frequency-domain photon-migration spectroscopy *J. Biomed. Opt.* **15** 017003

Durduran T and Yodh A G 2014 Diffuse correlation spectroscopy for non-invasive, micro-vascular cerebral blood flow measurement *NeuroImage* **85** 51–63

Durduran T *et al* 2010 Optical measurement of cerebral hemodynamics and oxygen metabolism in neonates with congenital heart defects *J. Biomed. Opt.* **15** 037004

Ferradal S L, Liao S M, Eggebrecht A T, Shimony J S, Inder T E, Culver J P and Smyser C D 2016 Functional imaging of the developing brain at the bedside using diffuse optical tomography *Cereb. Cortex* **26** 1558–68

Greisen G, Andresen B, Plomgaard A M and Hyttel-Sorensen S 2016 Cerebral oximetry in preterm infants: an agenda for research with a clear clinical goal *Neurophotonics* **3** 031407

Gurley K, Shang Y and Yu G 2012 Noninvasive optical quantification of absolute blood flow, blood oxygenation, and oxygen consumption rate in exercising skeletal muscle *J. Biomed. Opt.* **17** 075010

Hebden J C, Gibson A, Yusof R M, Everdell N, Hillman E M, Delpy D T, Arridge S R, Austin T, Meek J H and Wyatt J S 2002 Three-dimensional optical tomography of the premature infant brain *Phys. Med. Biol.* **47** 4155–66

Hinojosa-Rodriguez M, Harmony T, Carrillo-Prado C, Van Horn J D, Irimia A, Torgerson C and Jacokes Z 2017 Clinical neuroimaging in the preterm infant: diagnosis and prognosis *Neuroimage Clin.* **16** 355–68

Huang C, Gu Y, Chen J, Bahrani A, Jawdeh E G A, Bada H S, Saatman K, Yu G and Chen L 2019a A wearable fiberless optical sensor for continuous monitoring of cerebral blood flow in mice *IEEE J. Sel. Top. Quantum* **25** 1–8

Huang C, Irwin D, Lin Y, Shang Y, He L, Kong W, Luo J and Yu G 2015a Speckle contrast diffuse correlation tomography of complex turbid medium flow *Med. Phys.* **42** 4000–6

Huang C, Irwin D, Zhao M, Shang Y, Agochukwu N, Wong L and Yu G 2017 Noncontact 3-dimensional speckle contrast diffuse correlation tomography of tissue blood flow distribution *IEEE Trans. Med. Imaging* **36** 2068–76
Huang C, Lin Y, He L, Irwin D, Szabunio M M and Yu G 2015b Alignment of sources and detectors on breast surface for noncontact diffuse correlation tomography of breast tumors *Appl. Opt.* **54** 8808–16
Huang C, Mazdeyasna S, Chen L, Abu Jawdeh E G, Bada H S, Saatman K E, Chen L and Yu G 2019b Noninvasive noncontact speckle contrast diffuse correlation tomography of cerebral blood flow in rats *Neuroimage* **198** 160–9
Huang C, Radabaugh J P, Aouad R K, Lin Y, Gal T J, Patel A B, Valentino J, Shang Y and Yu G 2015c Noncontact diffuse optical assessment of blood flow changes in head and neck free tissue transfer flaps *J. Biomed. Opt.* **20** 075008
Hyttel-Sorensen S *et al* 2013 Clinical use of cerebral oximetry in extremely preterm infants is feasible *Dan Med. J.* **60** A4533
Hyttel-Sorensen S *et al* 2015 Cerebral near infrared spectroscopy oximetry in extremely preterm infants: phase II randomised clinical trial *BMJ* **350** g7635
Irwin D, Dong L X, Shang Y, Cheng R, Kudrimoti M, Stevens S D and Yu G 2011 Influences of tissue absorption and scattering on diffuse correlation spectroscopy blood flow measurements *Biomed. Opt. Express* **2** 1969–85
Jain V *et al* 2014 Cerebral oxygen metabolism in neonates with congenital heart disease quantified by MRI and optics *J. Cerebral Blood Flow Metab.* **34** 380–8
Kim M N *et al* 2010 Noninvasive measurement of cerebral blood flow and blood oxygenation using near-infrared and diffuse correlation spectroscopies in critically brain-Injured adults *Neurocrit Care* **12** 173–80
Kooi E M W, Verhagen E A, Elting J W J, Czosnyka M, Austin T, Wong F Y and Aries M J H 2017 Measuring cerebrovascular autoregulation in preterm infants using near-infrared spectroscopy: an overview of the literature *Expert Rev. Neurother.* **17** 801–18
Lin Y, Huang C, Irwin D, He L, Shang Y and Yu G 2014 Three-dimensional flow contrast imaging of deep tissue using noncontact diffuse correlation tomography *Appl. Phys. Lett.* **104** 121103
Lynch J M, Buckley E M, Schwab P J, Busch D R, Hanna B D, Putt M E, Licht D J and Yodh A G 2014 Noninvasive optical quantification of cerebral venous oxygen saturation in humans *Acad. Radiol.* **21** 162–7
Mazdeyasna S, Huang C, Zhao M, Agochukwu N B, Bahrani A A, Wong L and Yu G 2018 Noncontact speckle contrast diffuse correlation tomography of blood flow distributions in tissues with arbitrary geometries *J. Biomed. Opt.* **23** 096005
Naidech A M, Bendok B R, Ault M L and Bleck T P 2008 Monitoring with the Somanetics INVOS 5100C after aneurysmal subarachnoid hemorrhage *Neurocrit Care* **9** 326–31
Noori S and Seri I 2015 Hemodynamic antecedents of peri/intraventricular hemorrhage in very preterm neonates *Semin. Fetal Neonatal Med.* **20** 232–7
Park H K, Kim Y S, Oh S H and Lee H J 2015 Successful treatment with ultrasound-guided aspiration of intractable methicillin-resistant Staphylococcus aureus brain abscess in an extremely low birth weight infant *Pediatr. Neurosurg.* **50** 210–5
Scholkmann F, Kleiser S, Metz A J, Zimmermann R, Mata Pavia J, Wolf U and Wolf M 2014 A review on continuous wave functional near-infrared spectroscopy and imaging instrumentation and methodology *NeuroImage* **85** 6–27
Severdija E E, Vranken N P, Teerenstra S, Ganushchak Y M and Weerwind P W 2015 Impact of intraoperative events on cerebral tissue oximetry in patients undergoing cardiopulmonary bypass *J. Extra Corpor. Technol.* **47** 32–37
Shang Y, Cheng R, Dong L, Ryan S J, Saha S P and Yu G 2011 Cerebral monitoring during carotid endarterectomy using near-infrared diffuse optical spectroscopies and electroencephalogram *Phys. Med. Biol.* **56** 3015–32
Shang Y, Gurley K and Yu G 2013 Diffuse correlation spectroscopy (DCS) for assessment of tissue blood flow in skeletal muscle: recent progress *Anat. Physiol. Curr. Res.* **3** 128
Shang Y, Li T, Chen L, Lin Y, Toborek M and Yu G 2014 Extraction of diffuse correlation spectroscopy flow index by integration of *N*th-order linear model with Monte Carlo simulation *Appl. Phys. Lett.* **104** 193703
Shang Y, Zhao Y, Cheng R, Dong L, Irwin D and Yu G 2009 Portable optical tissue flow oximeter based on diffuse correlation spectroscopy *Opt. Lett.* **34** 3556–8
Underwood M A, Milstein J M and Sherman M P 2007 Near-infrared spectroscopy as a screening tool for patent ductus arteriosus in extremely low birth weight infants *Neonatology* **91** 134–9
Wang L, Li G, Adeli E, Liu M, Wu Z, Meng Y, Lin W and Shen D 2018 Anatomy-guided joint tissue segmentation and topological correction for 6-month infant brain MRI with risk of autism *Hum. Brain Mapp* **39** 2609–23
White B R, Liao S M, Ferradal S L, Inder T E and Culver J P 2012 Bedside optical imaging of occipital resting-state functional connectivity in neonates *Neuroimage* **59** 2529–38
Yu G, Durduran T, Furuya D, Greenberg J H and Yodh A G 2003 Frequency-domain multiplexing system for in vivo diffuse light measurements of rapid cerebral hemodynamics *Appl. Opt.* **42** 2931–9
Yu G, Floyd T F, Durduran T, Zhou C, Wang J, Detre J A and Yodh A G 2007 Validation of diffuse correlation spectroscopy for muscle blood flow with concurrent arterial spin labeled perfusion MRI *Opt. Express* **15** 1064–75
Yu G, Lin Y and Huang C 2016 Noncontact three-dimensional diffuse optical imaging of deep tissue blood flow distribution *US Patent* #9861319 (2016–2036)
Zaramella P, Freato F, Quaresima V, Ferrari M, Bartocci M, Rubino M, Falcon E and Chiandetti L 2006 Surgical closure of patent ductus arteriosus reduces the cerebral tissue oxygenation index in preterm infants: a near-infrared spectroscopy and Doppler study *Pediatr. Int.* **48** 305–12
Zhao J, Ding H S, Hou X L, Zhou C L and Chance B 2005 *In vivo* determination of the optical properties of infant brain using frequency-domain near-infrared spectroscopy *J. Biomed. Opt.* **10** 024028